IOP Conf. Series: Materials Science and Engineering **355** (2018) 012009 doi:10.1088/1757-899X/355/1/012009

Analysis of the impact of modification of cold crucible design on the efficiency of the cold crucible induction furnace

R Przylucki[1], S Golak[1], P Bulinski[2], J Smolka[2], M Palacz[2], G Siwiec[3], J Lipart[3] and L Blacha[3]

[1]Department of Industrial Informatics, Silesian University of Technology, Krasinskiego 8, 40-019 Katowice, Poland
[2] Institute of Thermal Technology Silesian, University of Technology, Konarskiego 22, 44-100 Gliwice, Poland
[3]Institute of Metals Technology, Silesian University of Technology, Krasinskiego 8, 40-019 Katowice, Poland

E-mail: roman.przylucki@polsl.pl

Abstract. The article includes numerical simulation results for two induction furnace with cold crucible (IFCC). Induction furnaces differ in cold crucible design, while the inductor geometry was preserved for both variants. Numerical simulations were conducted as three dimensional one, with coupled analysis of electromagnetic, thermal and fluid dynamics fields. During the experiment, six calculation variants, differ in amount of molten titanium (three different weights of titanium for each type of cold crucible) were considered. Main parameters controlled during the calculations were: electrical efficiency of the IFCC and the meniscus shape of liquid metal.

1. Introduction

Induction furnaces with cold crucible are most commonly used for melting very reactive metals and alloys. Such metals should be melted without contact with the crucible. Cold crucible is a compromise solution. The best, from the point of view of lack of contact, is the levitation melting. But in levitation melting there are problems with the lifting force especially for heavy workpieces. In cold crucible furnace, the molten metal contacts only with a bottom of the crucible. From the crucible walls, liquid metal is repulsed by electrodynamic forces. At the bottom, the metal is in contact with the crucible not directly, but through a solidified layer (skull). There are two main problems in cold crucible furnaces design: electric (and of course total) efficiency, and minimization of the skull [1].

Low electric efficiency is due to double conversion of electrical energy: from current to the electromagnetic field and again to current. First conversion between inductor and cold crucible segment (finger) and the second between cold crucible segments and the molten metal. This cannot be changed but energy losses can be reduced by the appropriate cold crucible construction [2]. Moreover, the skull volume depends on the cold crucible construction.

The aim of the article is the modification of the design of cold crucible to improve the efficiency of the melting process and to minimize the skull.

2. Models of considered cold crucibles

Two cold crucible designs are investigated in this article. Simplified sketch of the first and the second construction is presented in Figure 1 and 2, respectively. As shown in Figure 1 first construction was made from one piece of copper. There is a separation between segments, and the incision also includes part of the crucible bottom (orange part with index 6). There is a massive chassis below the inductor. The shuns does not have pole pieces. The crucible bottom is slightly concave. Advantage of this design is the incision of the outer part of bottom which prevents shorting of the currents induced in the bottom part of the segments. Disadvantages of this construction are: massive chassis just below the inductor, and lack of pole pieces. Problematic is also the recess in the bottom. This causes a thick skull.

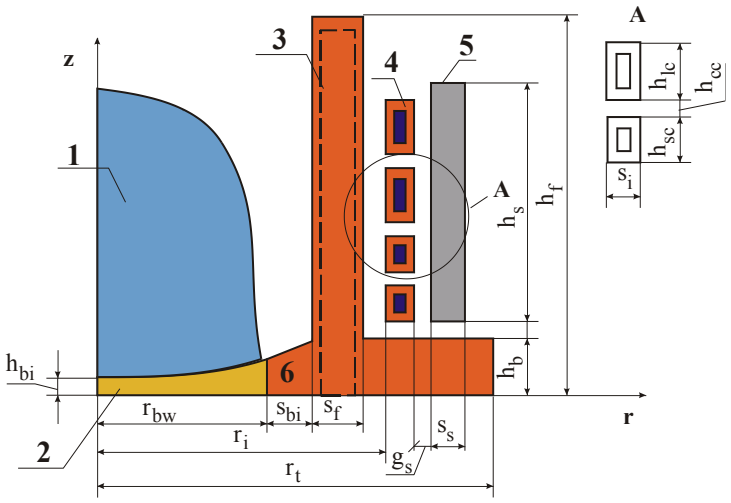

Figure 1. Sketch of first IFCC Model, 1 – metal melt, 2 – solid bottom, 3 – segment, 4 – inductor, 5 – shunt, 6 – separated part of the bottom.

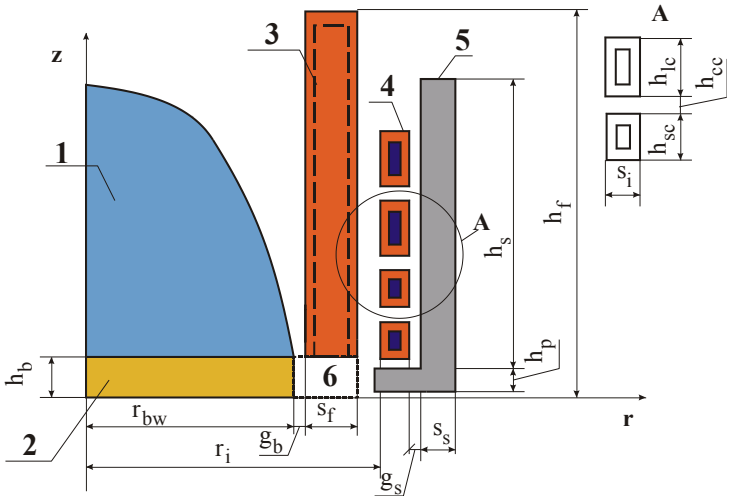

Figure 2. Sketch of second IFCC Model, 1 – metal melt, 2 – solid bottom, 3 – segment, 4 – inductor, 5 – shunt, 6 – ceramic element.

The second construction of the cold crucible, considered in this article, consists of two main, separate pieces: segments and flat bottom. The shunts has pole pieces below the inductor, and there is no conducting material just below inductor and segments. Such a design (more difficult from the construction point of view) prevents the induction of currents outside the cold crucible segments.

2.1. Model for electromagnetic field analysis

Analysis of electromagnetic field basis on A-V formulation equation (1) [3] is conducted as a steady state one. Electromagnetic field analysis results were volumetric heat sources equation (2) [4] and volumetric electromagnetic forces equation (4) [4]. These values were calculated in the melt area only, and they are input data for temperature and fluid dynamics analysis.

$$\mathrm{rot}\left(\frac{1}{\mu_0}\frac{1}{\mu}\mathrm{rot}\,\mathbf{A}\right)+\boldsymbol{\sigma}\left(\mathrm{j}\omega\mathbf{A}+\mathrm{grad}\,V\right)=0 \tag{1}$$

where:

μ_0 - permeability of vacuum; μ - relative permeability; **A** - magnetic vector potential; σ - conductivity; ω - angular velocity; V - scalar electric potential; j - unit imaginary number.

$$q_v=\frac{1}{2}|\mathbf{J}|^2\cdot\frac{1}{\sigma} \tag{2}$$

where: q_v - volumetric density of active power; **J** - current density.

$$\mathbf{J}=-\sigma\left(\mathrm{j}\omega\mathbf{A}+\mathrm{grad}\,V\right) \tag{3}$$

$$\mathbf{f}_m=\frac{1}{2}\Re\mathrm{e}\,(\mathbf{J}\times\mathbf{B}^*) \tag{4}$$

$$\mathbf{B}=\mathrm{rot}\,\mathbf{A} \tag{5}$$

where:

$\mathbf{f}_m$ - time average for period volumetric force density; **B*** - conjugate value of induction.

The problem was considered as coupled analysis of: electromagnetic, thermal and fluid dynamics fields in 3-D domain. Electromagnetic field analysis was performed with use of getDP program [5]. For the temperature and fluid dynamics analysis, Ansys-Fluent program was used.

For electromagnetic field calculation, only 1/16 of the device was modelled (Figure 3). It was possible because of periodicity of the device construction.

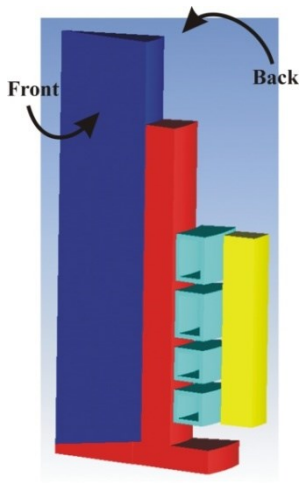

Figure 3. Calculation model for electromagnetic field analysis of the first IFCC.

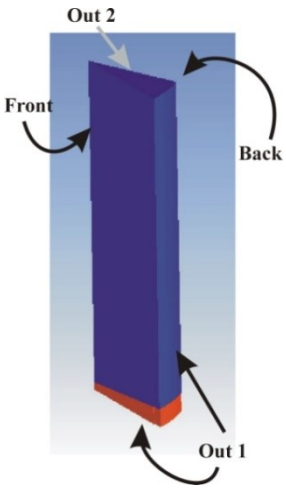

Figure 4. Calculation model for thermal and fluid dynamics field analysis of the first IFCC.

On front and back model surfaces (Figure 3), the periodicity boundary condition was applied. In other directions, the computational model is surrounded by air and on the outside air surfaces boundary Dirichlet condition setting potentials to zero was applied.

Basic dimensions of the models are presented in Table 1. Bottom and segments of crucible were made of copper of the conductivity of $56 \cdot 10^6$ S/m, melt metal was made of titanium with the conductivity of $50.5 \cdot 10^4$ S/m. Shunts were made of Fluxtrol 100.

Table 1. Model parameters.

Parameter (mm)	Model 1	Model 2
r_{bw}	40	45
s_{bi}	6	1
s_f	15	15
g_s	2	2
s_s	10	10
s_i	13	13
r_i	75	75
r_t	90	-
h_{bi}	4	10
h_b	10	10
h_s	85	85
h_p	-	7.5
h_f	144	144
h_{sc}	3	13
h_{lc}	25	25
h_{cc}	4	4

2.2. Model for temperature field and fluid dynamics analysis

Analysis of temperature field and fluid dynamics were performed in Ansys Fluent program. The calculation domain was limited to the melt area and a bottom of crucible only, as presented in Figure 4. Temperature calculations were based on equation (6) [6].

$$\frac{\partial}{\partial t}\left(\rho c T\right) + \rho c \, \mathbf{v} \operatorname{grad} T = \operatorname{div}\left(k \operatorname{grad} T\right) + q_v + q_r \tag{6}$$

where:

ρ - density; c - specific heat; T - temperature; **v** – velocity vector; k - thermal conductivity; q_v - volumetric heat source from electromagnetic calculation; q_r - volumetric density of radiative heat exchange derived on the basis of Gauss-Ostrogradsky theorem from surface radiative heat transfer [7].

As in the case of electromagnetic field analysis, the calculation domain was limited to 1/16 of the device (Figure 4). On the front and back model surfaces adiabatic boundary condition was applied, on the outside surface in the crucible segments and below bottom (out 1, Figure 4.) Dirichlet boundary condition setting temperature to 303 K was applied, on the free molten metal surface (out 2), the heat loss with convection and radiation were taken into consideration.

The fluid dynamics calculations should determine the shape of free surface of molten metal in the IFCC and therefore the flow field within crucible was treated as multiphase one. The Volume of Fluid approach was applied in the calculation model. To obtain the flow field distribution, the continuity equation in the form equation (7) [6] and momentum conservation equation (8) [6] should be solved.

$$\frac{\partial}{\partial t}\left(\alpha_q \rho_q\right) + \operatorname{div}\left(\alpha_q \rho_q \mathbf{v}\right) \tag{7}$$

where: α_q - volume fraction of the q^{th} phase; ρ_q - density of the q^{th} phase.

$$\frac{\partial}{\partial t}\left(\rho \mathbf{v}\right) + \operatorname{div}\left(\rho \mathbf{v}\mathbf{v}\right) = -\operatorname{grad} p + \varepsilon\left(\operatorname{grad}\operatorname{div}\mathbf{v} - \operatorname{rot}\operatorname{rot}\mathbf{v}\right) + \rho\mathbf{g} + f_m + f_s \tag{8}$$

where: p - pressure; ε - dynamic viscosity; **g** - gravitational acceleration; f_s - volume force density calculated from surface tension derived on the basis of Gauss-Ostrogradski theorem [8].

These equations are supplemented with boundary condition, on the front and back surfaces periodicity boundary condition was assumed. On the top of model pressure outlet condition was adopted, for the free surface of molten metal shear stress equal to 0 on both sides was assumed. On the outside wall of the model (out 2), no slip condition was assumed.

2.3. Coupling procedure

Electromagnetic, heat transfer and fluid flow calculation were conducted for two different numerical submodels. Models differs in geometry and calculation domain. Calculation model for electromagnetic field consists of molten metal, crucible, inductor, shunt and air. Temperature and fluid dynamic calculations were conducted for the model limited to the molten metal and air above free surface of metal, and bottom of the crucible.

Fluid dynamics and temperature calculations were performed in time domain, and the time step was 0.00001 s. Each 25 time steps the calculations of electromagnetic field were performed and mean for the period values of forces and power sources were determined, and then transferred as the source terms for the thermal submodel. Before the transfer, the forces and heat sources from electromagnetic calculation were approximated for the thermal - fluid dynamic calculation mesh [9].

3. Numerical experiment

Six simulation variants were performed during the experiment. For each of the two IFCC models, three calculation variants, different in volume of the titanium, were conducted. The variant designators are as follows: IFCC model 1, volume of titanium 1 is designated as m1v1. Considered quantities of titanium are: 1.06 kg, 1.6 kg, 2.13 kg which corresponds to complete filling the crucible to the level of 0.04 m (27%), 0.06 m (42%), 0.08 m (55%).

All variants of calculations were conducted for the same inductor current and current frequency of 10 kHz. The liquid metal properties were as follows: conductivity [10] $\sigma = 50.5 \cdot 10^4$ S/m density [11] $\rho = 4160$ kg/m^3, thermal conductivity [12] $\lambda = 32$ W/(m·K), specific heat $c = 9.87 \cdot 10^2$ J/(kg·K), dynamic viscosity [13] $\varepsilon = 4.03 \cdot 10^{-3}$ (Pa·s).

Due to the difficulty of coupling of the model to the electromagnetic field analysis with the model for temperature and FD field analysis, the calculations were made only partially. In the Figure 5, and Figure 6 calculation results for the m1v1 variant for two different supply powers 20% of the maximum power (40 kW) and 40% of the maximum power (80 kW) are shown. Figures 5 and 6 shows meniscus shape. As can be seen, for 20% of the power the liquid metal is not completely pushed away from the walls of the crucible, but for the 40% of the power the liquid metal is completely pushed away from the wall of the crucible practically from the bottom of the IFCC. But at this stage of the calculations, no metal solidification has yet be taken into account.

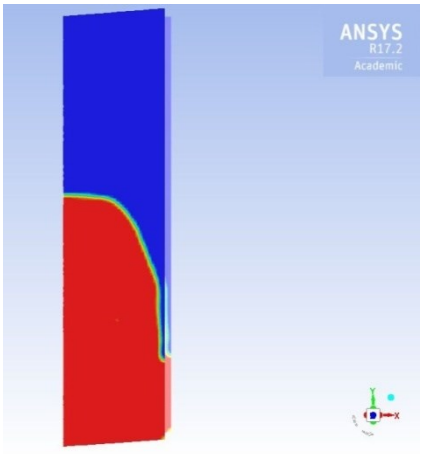

Figure 5. Metal meniscus shape for 20% of the supply power.

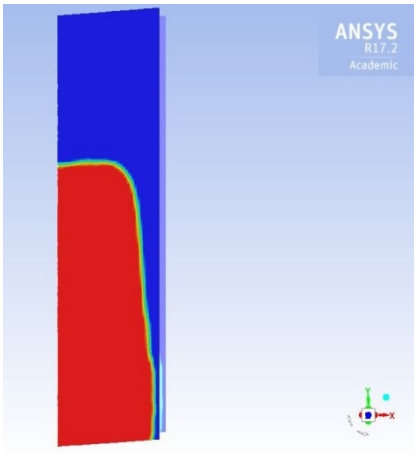

Figure 6. Metal meniscus shape for 40% of the supply power.

References

[1] Spitans S, Baake E, Jakovics A and Franz H 2015 Numerical simulation of electromagnetic levitation in cold crucible furnace *Magnetohydrodynamics* **51** 567-578
[2] Rot D, Jirinec S, Kozeny J and Poznyak I 2015 Electrical efficiency of induction furnace with cold crucible via different segments width *Electric Power Engineering (EPE) 16th International Conference* IEE DOI 10.1109/EPE.2015.7161132
[3] Fort J, Garnich M and Klymyshyn N 2005 Electromagnetic and thermal-flow modelling of a cold-wall crucible induction melter *Metallurgical and Materials Transaction B* **36** 141-152
[4] Flux 2005 *3D Vol5 Complement on the formulations 3D* Cedrat 138-171.
[5] Dular P, Geuzaine C *GetDP reference manual: the documentation for GetDP, a general environmental for the treatment of discrete problems* getdp.info
[6] *Ansys 15.0 manual* www.ansys.com
[7] *Fluent 6.3 User's Guide 13.2.1 Heat transfer theory* https://www.sharcnet.ca/Software/Fluent6/html/ug/node568.htm
[8] *Fluent 6.3 User's Guide 23.3.8 Surface Tension and Wall Adhesion* https://www.sharcnet.ca/Software/Fluent6/html/ug/node888.htm
[9] Bulinski P, Smolka J, Golak S, Przylucki R, Palacz M, Siwiec G, Lipart J, Bialecki R and Blacha L 2017 Numerical and experimental investigation of heat transfer process in electromagnetically driven flow within vacuum induction furnace *Applied Thermal Engineering* **124** 1003-13
[10] Seydel U and Fucke W 1980 Electrical resistivity of liquid Ti, V, Mo and W *Journal of Physics F: Metal Physics* **10**
[11] Ishikawa T 2005 Thermophysical properties of molten refractory metals measured by an elecrostatic levitator *Journal of Electric Materials*
[12] Mills K, Monaghan B and Knee J 1996 Thermal conductivities of liquid metals *Proceedings of the Twenty-Third International Thermal Conductivity Conference*
[13] Pardis P, Ishikawa T and Yoda S 2002 Non contact measurements of surface tensions and viscosity of niobium, zirconium and titanium using and electrostatic levitation furnace *International Journal of Thermophysics* **23**

Acknowledgments

Financial assistance was provided by grant no. 2014/13/B/ST8/02364 funded by the National Science Centre, Poland, and is here acknowledged.